# POLAR CEPPAD/IPS ENERGETIC NEUTRAL ATOM (ENA) IMAGES OF A SUBSTORM INJECTION

M. G. Henderson*, G. D. Reeves*, A. M. Jorgensen*, H. E. Spence†, L. A. Frank‡, J. B. Sigwarth‡ J. F. Fennell§, J. L. Roeder§, J. B. Blake§, K. Yumoto¶, and S. Bourdarie‖

*Los Alamos National Laboratory, Los Alamos, New Mexico, USA
†Center for Space Physics Research, Boston University, Boston, Massachusetts, USA
‡Physics and Astronomy Department, University of Iowa, Iowa City, Iowa, USA
§The Aerospace Corporation, El Segundo, California, USA
¶Department of Earth and Planetary Sciences, Kyushu University, Japan
‖ONERA, Centre d'Études et de Recherches de Toulouse, France

## ABSTRACT

The CEPPAD Imaging Proton Spectrometer on the POLAR spacecraft has proven to perform very well as an Energetic Neutral (ENA) atom imager, despite the fact that it was designed primarily for measuring energetic ions *in-situ.* ENAs emitted from the ring current can be detected during storm- as well as quiet-time conditions and can be monitored continuously for many hours at a time when Polar is situated in the polar cap. In addition, we are able to routinely detect 'bursts' of ENA emissions in response to substorm-associated ion injections. In this paper, we present ENA images of a single such event together with global auroral imager data from the POLAR VIS instrument, LANL geosynchronous energetic particle data, and ground magnetic Pi2 data in order to establish that such bursts are indeed caused by substorm injections.

## INTRODUCTION

Energetic neutral atoms (ENAs) are created in the inner magnetosphere when charge exchange collisions occur between energetic ions and the cold neutral population of the earth's tenuous extended atmosphere. Because gravitational forces are negligible for typical energies of interest and they are unaffected by the earth's electric and magnetic fields, ENAs travel in approximately straight line trajectories away from the charge-exchange sites and carry with them valuable information about the pitch angle and energy distributions of the ion population from which they were emitted. Since these emissions can be detected remotely with an appropriately instrumented spacecraft, images of the charge exchange process can be constructed and used to probe the global ion distribution of the inner magnetosphere.

This powerful technique has been used successfully in the study of the stormtime ring current by several investigators (e.g. see: *Roelof et al.* [1985]; *Roelof* [1987]; *Chase and Roelof* [1995]; *Lui et al.* [1996]; *Wilken et al.* [1997]; *Henderson et al.* [1997]; *Barabash et al.* [1997]; *C:son Brandt et al.* [1997]; *Jorgensen et al.* [1998] and *Henderson et al.* [1998]). The spatial and/or temporal variability of the ring current can be studied on a global scale. Ring current asymmetries can be determined. And the global equatorial ion distribution can be extracted from the images via forward modeling techniques. Furthermore, the long timescale of storms allows for relatively long integration times to be used in order to build up acceptable counting statistics.

However, another important contributor to changes in the inner magnetospheric ion population (during both storm and non-storm intervals) are individual substorm injections which have much shorter times scales. As pointed out by *Daglis and Livi* [1995], the ability to image these injections on a global scale with ENAs would provide a revolutionary

way of addressing some of the currently unresolved problems relating to substorm physics. Unfortunately, imaging substorms is more problematic than imaging the ring current for two main reasons: 1) injections are expected to occur farther from the earth where the neutral density and hence the ENA emission rate is lower and 2) substorms occur on a much shorter timescale than do storms and so shorter integration times are necessary as well.

Despite these complications, we find that with the POLAR CEPPAD/IPS instrument, we are routinely able to detect ENA bursts in response to substorm-associated ion injections measured at geosynchronous orbit (e.g. see *Henderson et al.* [1997] and *Jorgensen* [1998]). In this paper, we present POLAR ENA images acquired on November 24, 1996 together with POLAR VIS imagery, ground magnetometer data, and geosynchronous energetic particle data in order to verify that such ENA bursts are indeed due to substorm injections.

## INSTRUMENTATION

The energetic neutral atom images presented here were acquired with the Imaging Proton Spectrometer (IPS) on the Polar spacecraft. The IPS is one of four instruments that make up the Comprehensive Energetic Particle and Pitch Angle Distribution experiment (CEPPAD). The other CEPPAD instruments are: the Imaging Electron Spectrometer (IES), the High-Sensitivity Telescope (HIST) and the Source/loss-cone Energetic Particle Spectrometer (SEPS). The IPS instrument is designed to detect protons with energies in the range 13.9-1500 keV in 16 energy channels over 9 separate look-directions simultaneously. The nine detectors are arranged to be at the polar angles $10^\circ$, $30^\circ$, $50^\circ$, $70^\circ$, $90^\circ$, $110^\circ$, $130^\circ$, $150^\circ$, and $170^\circ$ with respect to the spacecraft spin axis, and each has an instantaneous field of view of $20^\circ$ in the polar direction by $11.25^\circ$ in the azimuthal direction for a total instantaneous field of view of $180^\circ \times 11.25^\circ$. A full coverage of the unit sphere is therefore obtained once every 6 second spin.

Although designed to measure ions *in-situ*, the IPS also detects energetic neutrals with a high efficiency. But since the instrument was not designed to distinguish between charge states, ENAs can only be reliably identified when Polar is situated in the polar caps where the ambient flux of energetic ions is usually very low. Due to the $2 \times 9\mathrm{R_E}$ polar orbit of the Polar spacecraft, this condition is typically satisfied for many hours during each $\approx$ 18 hour orbit.

Two instrumental properties that affect the analysis of both energetic ions and energetic neutrals are: 1) the detector's sensitivity to earth and sun light and 2) the 'smearing' introduced by finite integration times combined with the spin of the spacecraft. Both of these artifacts are relatively minor problems when one is concerned with the *in-situ* measurement of ions because the ion pitch angle distributions do not tend to be highly anisotropic (although 'bursts' of energetic ions detected in the polar caps can be). Therefore, even when the light-contaminated data are removed, the ion pitch angle distributions are still very well determined. For energetic neutral atom detection, these artifacts must also be corrected for because ENAs tend to be highly directional and they come from directions close to the light-contaminating earth. In constructing ENA images from the IPS data, the light-contaminated pixels are 'blanked out', and for quantitative analysis (e.g. inversion of ENA images to extract the equatorial ion distributions), detailed knowledge of the angular response of the spinning instrument is required. For additional information concerning these and other instrumental issues see *Blake* et al. [1995], *Henderson et al.* [1997], and *Henderson et al.* [1998].

In this study, we present only data from the $E > 17.5$keV integral energy channel because it has good counting statistics and is sectored (on-board Polar) at the highest spatial resolution – 16 sectors per spin for the $10^\circ$ and $170^\circ$ detectors and 32 sectors per spin for the other detectors.

## OBSERVATIONS

In figure 1 we present the Polar CEPPAD/IPS ENA survey plot for November 24, 1996. The upper 9 panels on the lefthand side of the figure are 16-spin (96 s) averaged integral energy channel ($E > 17.5$ keV) sector versus time plots for each of the 9 IPS detectors. The data are shown in counts per second and are color-coded according to the color bar at the upper right of the plot. Plotted in the lower panel on the lefthand side are the 75-113 keV proton fluxes (on a linear scale in arbitrary units) from the Los Alamos National Laboratory geosynchronous energetic particle detectors on satellites 1994-084 (orange) and 1991-080 (purple). The universal time, radial distance, L-shell value, magnetic local time, magnetic latitude, and corrected magnetic latitude are indicated for various times at the bottom of this panel.

Shown on the righthand side of figure 1 from top to bottom are: the $D_{st}$ and the 6-hour averaged $K_p$ indices for a

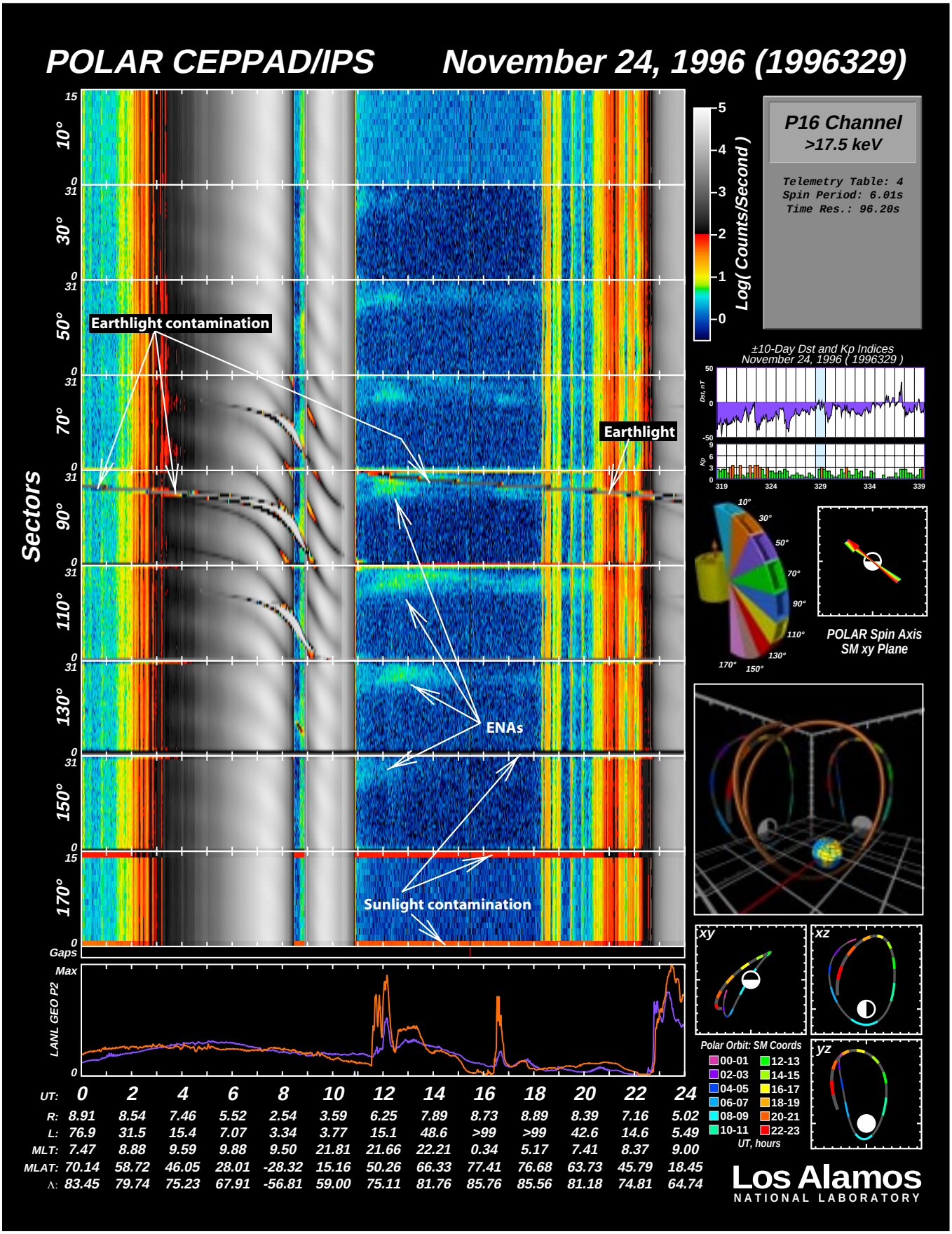


Figure 1: Substorm-associated energetic neutral atoms, November 24, 1996. Sector vs. time plots are shown in the 9 upper left panels (one for each look direction). The 75-113 keV differential proton channel from two LANL geosynchronous detectors are shown in the bottom left panel (linear scale, arb. units). Also shown are: the $D_{st}$ and $K_p$ indices, a schematic of the IPS look directions relative to the spacecraft, the spin axis projected onto the SM $xy$ plane, and some panels showing the orbit of Polar on this day. The substorm of interest occurred at approx. 1130 UT.

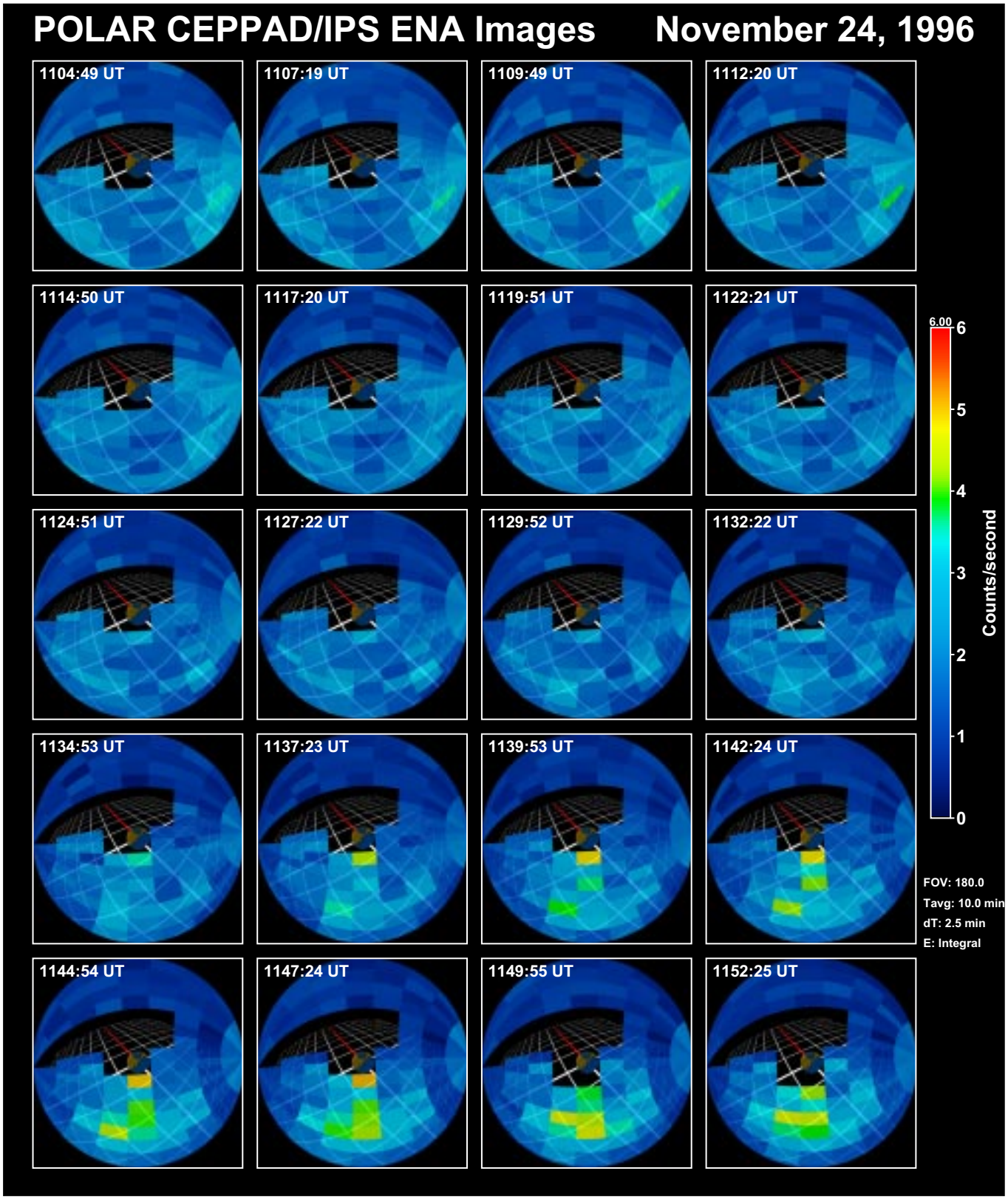


Figure 2: Energetic neutral atom images of a substorm injection that occurred on November 24, 1996. The $2 \times 2\mathrm{R_E}$ white grid represents the SM $xy$ plane ($+\hat{z}$ is up and $+\hat{x}$ is shown as a red line). The images are 10 minute averages and are shown in a $180^\circ$ fisheye projection.

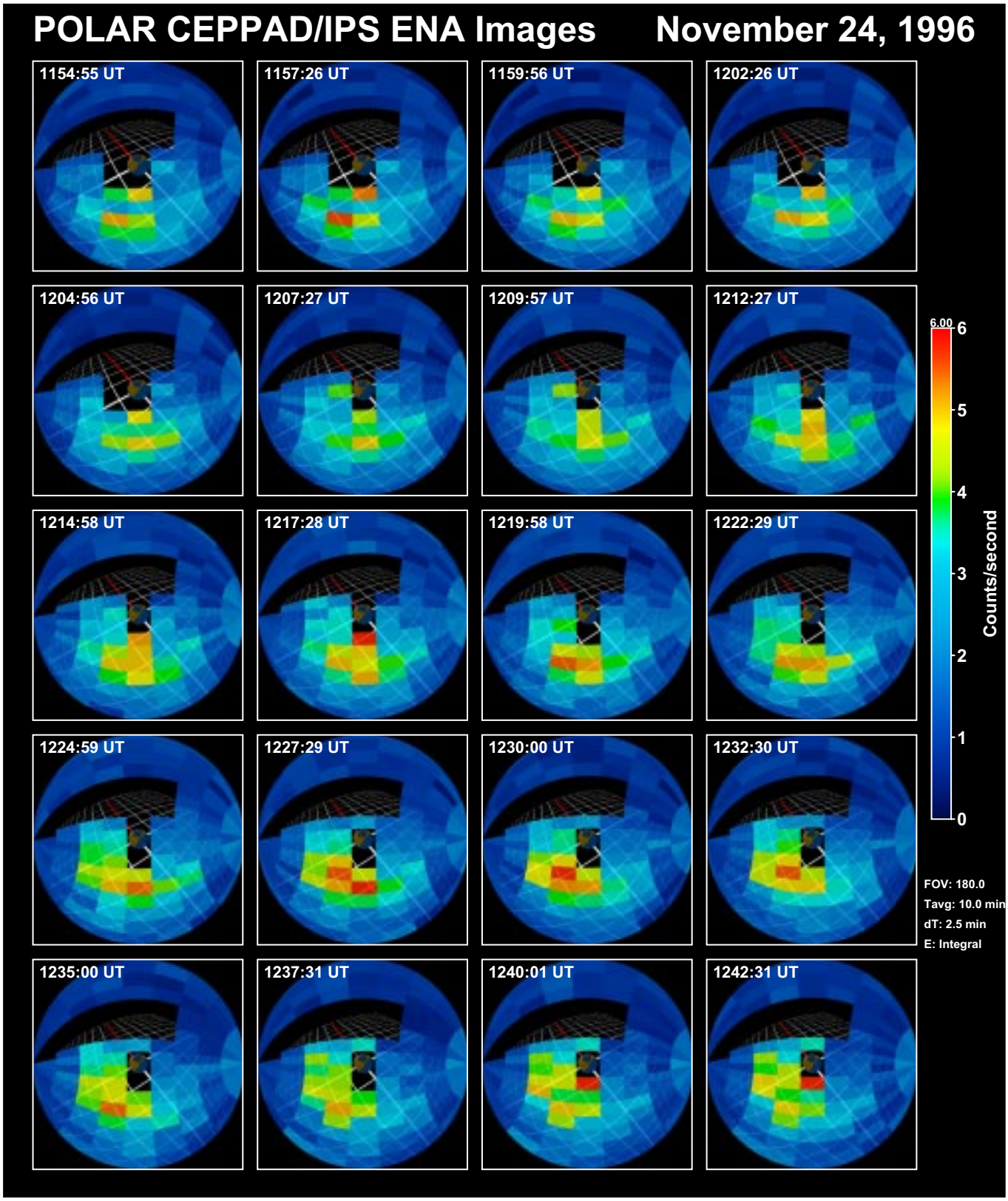


Figure 3: Continuation of figure 2.

21-day period centered on November 24, 1996; a schematic showing how the 9 IPS look-directions are oriented with respect to the Polar spin axis; the direction of the spin axis in the $xy$ plane of the Solar Magnetic (SM) coordinate system; a three-dimensional rendering of the Polar orbit in SM coordinates (the trajectory starts near apogee); and the Polar orbit projected onto the SM $xy$, $xz$, and $yz$ planes, color coded according to UT. (The white semi-circles represent the sun-light portion of the Earth.)

At the beginning of the day, Polar is situated high in the pre-noon sector of the northern polar cap near apogee on its way down toward a southern polar cap perigee pass (see the orbit plot panels in figure 1). The pre-noon ring current/radiation belt ions were encountered between approximately 0200 - 0800 UT, the southern polar cap at around 0830 UT, and the evening sector ring current/radiation belt ions between approximately 0900 - 1050 UT. The spacecraft then entered the northern polar cap shortly before 1100 UT and remained there for many hours until the pre-noon ring current/radiation belt ions were encountered again.

Between approximately 1050 - 1820 UT, the count rates in the polar cap drop to very low values indicating the absence of energetic ions at any significant flux levels. However, some highly directional horizontally inclined 'fuzzy' bands can be seen superimposed on the very low level background in this region. These are ENAs coming from look directions that pass close to the earth. Also seen throughout the day (but most clearly in the polar cap) are discrete lines or tracks due to earth and sun light contamination. The earth track can be seen in the $90^\circ$ detector (as a curved line) and the sun can be seen (as straight horizontal lines) in the highest and lowest sectors in the $70^\circ$ - $170^\circ$ detectors. Although the earth light ruins some of the ENA data, it nevertheless provides a convenient reference line that indicates the position of the earth on the ENA survey plots. As can be seen, the diffuse ENA emissions are clustered near the earth light track in the $90^\circ$ detector.

The LANL geosynchronous energetic proton data show that three main intervals of substorm injection activity occurred during this day: between 1100-1400 UT, between 1600-1800 UT, and after 2200 UT. The first two of these injections occurred while Polar was in the polar cap and we can see from the sector versus time plots in figure 1, that they were both accompanied by clear enhancements of the ENAs measured by IPS. From the $D_{st}$ index, it is clear that the enhanced ENA emissions are not the result of a storm-time buildup of the ring current, but are rather due to non-stormtime isolated substorm injections. (Note, however, that we can see an ENA enhancement in response to almost every observed geosynchronous proton injection, regardless of the pre-existing state of the ring current.)

In figures 2 and 3, we present a sequence of ENA images constructed from the IPS data for the time period between 1104:49–1242:31 UT during the first large proton injection observed at geosynchronous orbit. The images are 10 minute averages with center-time separations of 2.5 minutes (i.e. they are running averages). The projections for each image are $180^\circ$ fisheye views looking from the position of Polar (which was situated in the pre-midnight sector of the northern polar cap) toward the center of the earth. The white $2 \times 2$ $\mathrm{R_E}$ grid in each image represents the $xy$ plane of the SM coordinate system (its distortion shows the effect of the fisheye projection used) with the $+x$ axis shown as a red line. The sun is therefore located in the upper left of each figure (recall that in the SM coordinate system, the sun lies in the $xz$ plane and the dipole axis lies along the $+\hat{z}_{SM}$ axis, so the sun vector, $\hat{s}$, will be offset from the $+\hat{x}_{SM}$ axis by the geodipole tilt angle, which for 12UT on November 24, 1996 was -$16.4^\circ$). For all images, the earth- and sun-light contaminated pixels have been blanked out and are represented as fully transparent regions (the earth and the white SM $xy$ grid can be seen unattenuated in these regions).

The onset of the ENA enhancement is first clearly visible in the image taken at 1134:53 UT which is consistent with the time of the injection observed by the LANL geosynchronous detectors. The onset occurred in the pre-midnight sector with the enhanced ENA emissions coming from look directions that pass through the SM $xy$ plane inside of 8 $\mathrm{R_E}$. In many of the images, two distinct bright regions can be seen – one at very low altitudes adjacent to the southern part of the earth and another farther out that peaks in intensity between approximately 4-6 $\mathrm{R_E}$. Based on detailed modeling of ENA emissions from the inner magnetosphere under typical conditions, this morphology is entirely expected (e.g. see *Williams et al.* [1992]). The inner peak results from charge exchange collisions occurring between the dense low-altitude exosphere and the 'horns' of the magnetospheric ion population. The outer peak results more from charge exchange between the outer exosphere and the distributed inner magnetospheric ion population on the same set of flux tubes. And the entire distribution of ENA emissions is significantly affected by line-of-sight projection effects.

From figures 2 and 3, we can also see a clear westward drift of emissions from the onset region in the pre-midnight

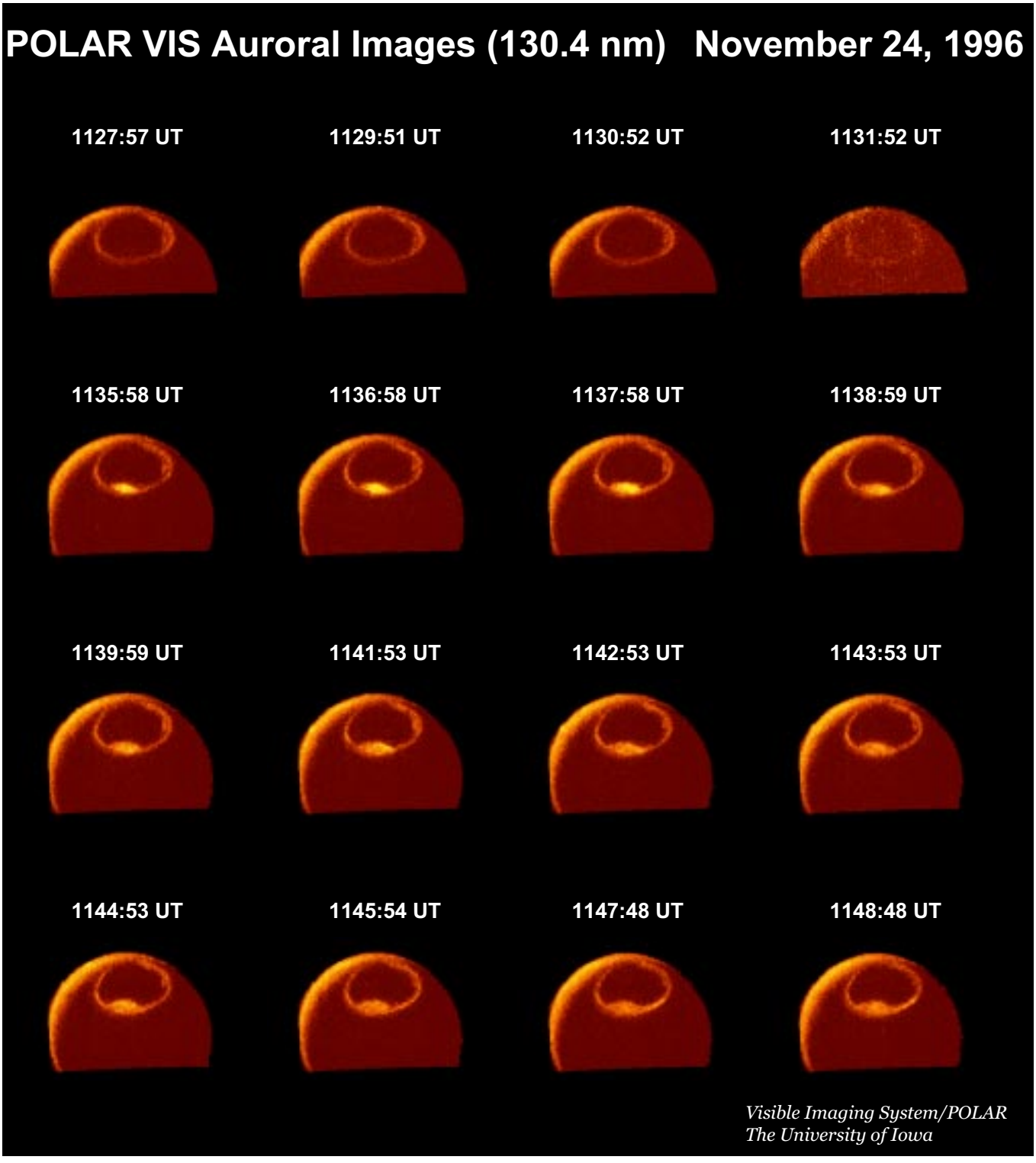


Figure 4: Development of the northern auroral distribution during the substorm as recorded by the POLAR VIS instrument. Onset must have occurred between 1131:52 UT and 1135:58 UT.

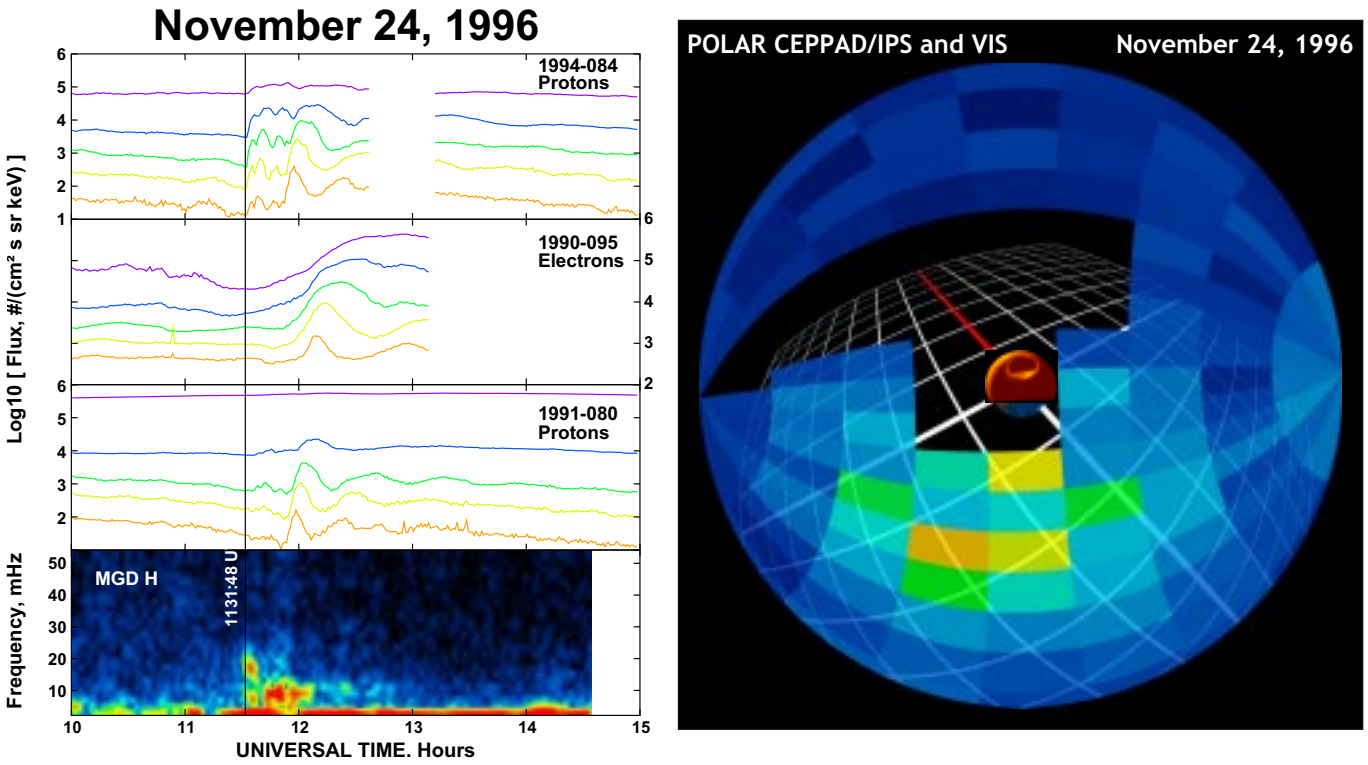


Figure 5: a) Los Alamos National Laboratory geosynchronous energetic particle data together with a frequency vs. time plot of the amplitude (of the envelope) of pulsations at Magadan. Onset is estimated to be 1131:48 UT. b) A composite image showing the an ENA and VIS image together on a single plot. The ENA image has a center time of 1159:56 UT and the VIS image was taken at 1159:05 UT.

sector around the earth toward the dayside. Although measuring the drift period directly from the integral energy images presented here is difficult due to the smearing introduced by energy dispersion effects, we can crudely estimate that it takes the faster ions (that we remotely sense via ENA emissions) about an hour to drift half way around the earth. This is consistent with proton energies on the order of 50keV and falls well within the energy range that we should be sensitive to.

In order to verify that this event was indeed a substorm and to obtain a more precise estimate of the onset time, we present additional data sets in figures 4 and 5. In figure 4, we present a sequence of auroral images acquired by the POLAR VIS instrument between 1127:57 UT and 1148:48 UT. From this plot we can see a very clear onset signature in the pre-midnight sector of the auroral oval in the image taken at 1135:58 UT followed by a classically expanding auroral substorm bulge. The onset must have occurred between 1131:52 UT and 1135:58 UT.

Shown in figure 5a are: the five lowest energy differential channels from the LANL energetic proton detectors on the geosynchronous satellites 1994-084 and 1991-080; the five lowest energy channels from the LANL energetic electron detectors on the geosynchronous satellite 1990-095; and an H-component frequency versus time spectrogram from the Magadan magnetometer station (part of the $210^\circ$ array – see *Yumoto* et al. [1996] for more information). From the dispersionless proton injection observed at 1994-084 and the Pi2 pulsations observed at Magadan, we estimate that onset occurred at 1131:48 UT ($\pm 30$ seconds). This time is consistent with the onset times derived from both the POLAR VIS data and from the POLAR CEPPAD/IPS ENA images.

## DISCUSSION AND SUMMARY

With the POLAR CEPPAD/IPS instrument, we routinely detect bursts of ENA emissions in association with substorm activity as illustrated by the two cases shown in figure 1. In this paper, we have presented ENA images for the first of these events along with POLAR VIS global auroral imager data, high-resolution ground magnetometer data, and Los Alamos National Laboratory energetic particle data. A composite image showing the spatial distribution of ENA emissions from the inner magnetosphere together with the global auroral distribution shortly after onset is presented

in figure 5b. From the datasets presented here, we find that: 1) the start of the ENA burst is consistent with the substorm onset time; 2) the onset of ENA emissions begins in the pre-midnight sector; and 3) the ENA emissions drift westward around the earth with drift periods consistent with ions having energies in the range of tens of keV and up. We therefore conclude that the ENA bursts are in fact charge exchange neutrals resulting from the injection of energetic particles into the inner magnetosphere during substorms.

As usual, it is important to bear in mind that ENA images do not map out the distribution of energetic ions directly, but rather they map out the distribution of charge-exchange neutrals resulting from the combination of the energetic ions and atmospheric neutrals. In order to recover the equatorial ion distribution alone, detailed modeling is required. In future studies, we will develop models and techniques to do this. But, as we have demonstrated in the present study, analysis of raw ENA images can also be very fruitful. The situation is crudely analogous to auroral imaging, where the intensity of auroral emissions do not directly map out the magnetospheric particle populations either – raw auroral imagery is nevertheless extremely valuable in its own right.

Having demonstrated that the POLAR CEPPAD/IPS instrument is capable of imaging substorm injections on a reasonable time scale, we can now apply this powerful technique to study a number of substorm-related issues. These include: the relationship between storms and substorms; the relative importance of the ring current as a substorm energy sink; the morphology of substorm ion injections; search for injection boundaries; dynamics of injection fronts; and superposed epoch studies. In addition, the ENA imagery acquired with the IPS instrument during storms and substorms can and will provide a global framework for the single point *in-situ* measurements being taken by the numerous ISTP-era spacecraft.

**ACKNOWLEDGEMENTS**

We gratefully acknowledge the following key scientists and engineers who contributed significantly to the IPS instrument: S. Imamoto, B. Johnson, W. A. Kolasinski, D. Mabry, J. Osborn, J. Skinner, F. Hilsenrath, C. Wilbur. This work was partially supported under NASA grant number S19511E. Work at Boston University was supported by NASA contract NAS5-97147. We also wish to thank K. Shiokawa (Solar-Terrestrial Environment Laboratory, Nagoya University, Japan) for processing, and providing on-line access to the $210^\circ$ MM magnetometer data.

## References

Barabash, S., P. C:son Brandt, O. Norberg, R. Lundin, E. C. Roelof, C. J. Chase, B. H. Mauk, and H. Koskinen, Energetic neutral atom imaging by the Astrid microsatellite, *Adv. Space Res., 20(#4-5)*, 1055–1060, 1997.

Blake, J. B., *et al.*, CEPPAD experiment on POLAR, *Space Sci. Rev.*, *71*, 531, 1995.

Chase, C. J., and E. C. Roelof, Extracting evolving structures from global magnetospheric images via model fitting and video visualization, *Johns Hopkins APL Technical Digest*, *16*, 111, 1995.

C:son Brandt, P., S. Barabash, , O. Norberg, R. Lundin, E. C. Roelof, C. J. Chase, B. H. Mauk, and M. F. Thomsen, ENA imaging from the Swedish microsatellite Astrid during the magnetic storm of 8 February, 1995, *Adv. Space Res., 20(#4-5)*, 1061–1066, 1997.

Daglis, I. A., and S. Livi, Potential merits for substorm research from imaging of charge-exchange neutral atoms, *Annales Geophysicae*, *13*, 505–516, 1995.

Henderson, M. G., G. D. Reeves, H. E. Spence, R. B. Sheldon, A. M. Jorgensen, J. B. Blake, and J. F. Fennell, First energetic neutral atom images from Polar, *Geophys. Res. Lett.*, *24*, 1167–1170, 1997.

Henderson, M. G., G. D. Reeves, K. R. Moore, H. E. Spence, A. M. Jorgensen, J. F. Fennell, J. B. Blake, and E. C. Roelof, Energetic neutral atom imaging with the Polar CEPPAD/IPS instrument: Initial forward modelling results, *Physics and Chemistry of the Earth, in press*, 1998.

Jorgensen, A. M., Global dynamics of the hot plasma in the inner magnetosphere: Energetic neutral atom (ENA) and in-situ measurements, Ph.D. thesis, Boston University, 1998.

Jorgensen, A. M., H. E. Spence, M. G. Henderson, G. D. Reeves, M. Sugiura, and T. Kamei, Global energetic neutral atom (ENA) measurements and their association with the $D_{st}$ index, *Geophys. Res. Lett.*, *24*, 3173–3176, 1998.

Lui, A. T. Y., D. J. Williams, E. C. Roelof, R. W. McEntire, and D. G. Mitchell, First composition measurements of energetic neutral atoms, *Geophys. Res. Lett.*, *23*, 2641, 1996.

Roelof, E. C., Energetic neutral atom image of a storm-time ring current, *Geophys. Res. Lett.*, *14*, 652, 1987.

Roelof, E. C., D. G. Mitchell, and D. J. Williams, Energetic neutral atoms ($E \approx 50$ keV) from the ring current: IMP 7/8 and ISEE 1, *J. Geophys. Res.*, *90*, 10991, 1985.

Wilken, B., I. A. Daglis, A. Milillo, S. Orsini, T. Doke, S. Livi, and S. Ullaland, Energetic neutral atoms in the outer magnetosphere: An upper limit obtained with the HEP-LD spectrometer on board GEOTAIL, *Geophys. Res. Lett.*, *24*, 111, 1997.

Williams, D. J., E. C. Roelof, and D. G. Mitchell, Global magnetospheric imaging, *Rev. Geophys.*, *30*, 183, 1992.

Yumoto, K., *et al.*, The STEP $210^\circ$ magnetic meridian network project, *J. Geomag. Geoelectr.*, *48*, 1297–13095, 1996.